HHS Public Access

Author manuscript

Brain Behav Immun. Author manuscript; available in PMC 2018 August 01.

Published in final edited form as:

Brain Behav Immun. 2017 August ; 64: 152–161. doi:10.1016/j.bbi.2017.04.008.

Safety parameter considerations of anodal transcranial direct current stimulation in rats

Mark P. Jackson[a,b], **Dennis Truong**[b], **Milene L. Brownlow**[a,c], **Jessica A. Wagner**[a], **R. Andy McKinley**[a], **Marom Bikson**[b], and **Ryan Jankord**[a]

[a]711th Human Performance Wing, Air Force Research Laboratory, Wright Patterson AFB, OH 45433

[b]Department of Biomedical Engineering, The City College of The City University of New York, CDI Building, 85 St. Nicholas Terrace, New York, NY 10031

[c]Research Associateship Program, National Research Council, National Academies of Science, Washington DC 20001

Abstract

A commonly referenced transcranial Direct Current Stimulation (tDCS) safety threshold derives from tDCS lesion studies in the rat and relies on electrode current density (and related electrode charge density) to support clinical guidelines. Concerns about the role of polarity (e.g. anodal tDCS), sub-lesion threshold injury (e.g. neuroinflammatory processes), and role of electrode montage across rodent and human studies support further investigation into animal models of tDCS safety. Thirty-two anesthetized rats received anodal tDCS between 0–5 mA for 60 minutes through one of three epicranial electrode montages. Tissue damage was evaluated using hemotoxylin and eosin (H&E) staining, Iba-1 immunohistochemistry, and computational brain current density modeling. Brain lesion occurred after anodal tDCS at and above 0.5 mA using a 25.0 mm^2 electrode (electrode current density: 20.0 A/m^2). Lesion initially occurred using smaller 10.6 mm^2 or 5.3 mm^2 electrodes at 0.25 mA (23.5 A/m^2) and 0.5 mA (94.2 A/m^2), respectively. Histological damage was correlated with computational brain current density predictions. Changes in microglial phenotype occurred in higher stimulation groups. Lesions were observed using anodal tDCS at an electrode current density of 20.0 A/m^2, which is below the previously reported safety threshold of 142.9 A/m^2 using cathodal tDCS. The lesion area is not simply predicted by electrode current density (and so not by charge density as duration was fixed); rather computational modeling suggests average brain current density as a better predictor for anodal tDCS. Nonetheless, under the assumption that rodent epicranial stimulation is a hypersensitive model, an electrode current density of 20.0 A/m^2 represents a conservative threshold for clinical tDCS, which typically uses an electrode current density of 2 A/m^2 when electrodes are placed on the skin (resulting in a lower brain current density).

Corresponding Author: Ryan Jankord, PhD., Air Force Research Laboratory, 711th Human Performance Wing, Wright Patterson AFB, OH 45433, Office: 937-318-3144, Ryan.Jankord@us.af.mil.

Keywords

tDCS; Rat cortex; Direct Current Stimulation; Current density; tDCS Modeling; Microglia

1. Introduction

Transcranial direct current stimulation (tDCS) is a non-invasive method of brain stimulation used to modulate cortical excitability (Nitsche et al., 2000). Conventional tDCS applies a small amount (1-2 mA) of direct current to the scalp using large (25-35 cm^2) electrodes (Brunoni et al., 2012, Woods et al., 2016). Computational and animal models have shown that only a fraction of the applied current reaches the cortex, leading to neuronal polarization and excitability changes in the cortex (Datta et al., 2009a, Marquez-Ruiz et al., 2012, Rahman et al., 2013, Rohan et al., 2015) and hippocampus (Rohan et al., 2015). Given its ability to affect the function of cortical neurons, tDCS has been investigated for a variety of medical and augmentative applications, such as depression (Brunoni et al., 2011, Loo et al., 2012), motor rehabilitation (Edwards et al., 2009), speech rehabilitation (Baker et al., 2010, Fridriksson et al., 2011, Galletta et al., 2015), pain control (Fregni et al., 2006, Dasilva et al., 2012, Castillo-Saavedra et al., 2016), and working memory (Brunoni et al., 2014). tDCS is considered a safe and well tolerated technique when proper protocols are followed (Bikson et al., 2009, Kasschau et al., 2015, Nitsche et al., 2015, Gbadeyan et al., 2016, Palm et al., 2016, Woods et al., 2016). Nonetheless, as the application of tDCS becomes increasingly commonplace and indications for its use more widespread, additional work on tDCS safety is warranted for supporting basic dosing guidelines (Peterchev et al., 2012, Bikson et al., 2016).

Initial safety limitations for tDCS were based upon literature from other electrical brain stimulation techniques. Nitsche et al. discussed safety of tDCS (Nitsche et al., 2003) by referencing safety standards in which pulsating current was applied directly to brain tissue (Yuen et al., 1981, Agnew et al., 1987, McCreery et al., 1990, Merrill et al., 2005)). In 2009, Liebetanz et al. conducted a canonical study in rodents to better define the minimum dosage at which cortical tissue damage occurs during cathodal tDCS: 0.5 mA for a stimulation duration of 10 minutes (Liebetanz et al., 2009). The findings reported by Liebetanz are widely cited in tDCS literature and have served as a guide for clinical safety limits (Holland et al., 2012, Brunoni et al., 2013, Truong et al., 2013). Though not extensively tested, Liebetanz suggested the metric of average electrode current density (A/m^2), calculated as the applied current divided by the electrolyte-body contact area – corresponding in their electrode montage to 143 A/m^2 - along with electrode charge density (C/m^2), which multiplies current density by time, as two generalized safety parameters for dosing guidelines (Bikson et al., 2009).

Building upon this framework for rodent safety studies, other tDCS paradigms were evaluated for lesion induction in the mouse (Rueger et al., 2012, Pikhovych et al., 2016a, Pikhovych et al., 2016b), where the lowest current intensity that produced detectable cortical damage was 0.5 mA (220 A/m^2 electrode current density) for both anodal and cathodal tDCS groups (Pikhovych et al., 2016b). However, damage was not consistently observed for

0.5 mA cathodal and 1.0 mA anodal stimulation groups (Pikhovych et al., 2016a, Pikhovych et al., 2016b), which indirectly suggests a role for polarity. More recently, lesions have been reported at an anodal current intensity of 0.6 mA (47.8 A/m^2 electrode current density) (Gellner et al., 2016), suggesting the lesion threshold in rats may be lower than previously reported. Rodent studies evaluating tDCS safety through microglial analysis have shown microglial activation can occur after anodal or cathodal stimulation at 0.5 mA for 15 minutes (Rueger et al., 2012) (c.f. (Liebetanz et al., 2009). Microglial changes in morphology associated with neurodegeneration after anodal tDCS have been reported at current intensities as low as 0.4 mA (31.8 A/m^2 electrode current density) (Gellner et al., 2016).

Considering the available lesion safety data and the variations in polarity, animal size, and electrode area used across studies, the robustness of average electrode current density (or electrode charge density) as a generalized predictor of injury remains unclear, undermining the use of animal data to support clinical safety thresholds. Indeed, computational current models notably show brain current density is not simply a function of the electrode current density, but also anatomy and details of electrode size and position (Datta et al., 2009a, Miranda et al., 2009, Datta et al., 2012, Saturnino et al., 2015). Therefore, animal models of tDCS safety can benefit from being updated in regards to: 1) variation of stimulation polarity/dose (anodal vs. cathodal); 2) alternative indications of injury (Wachter et al., 2011, Rueger et al., 2012, Wong et al., 2014, Gellner et al., 2016); and 3) the suitability of electrode parameters to set a safety threshold given computational current models show brain current density is not a simple, linear function of the applied current or electrode current density (Datta et al., 2009a, Miranda et al., 2009, Datta et al., 2012, Saturnino et al., 2015).

We initially developed an *in vivo* rodent model of anodal tDCS using a 25.0 mm^2 electrode and evaluated the effect of various stimulation dosages on tissue damage. We evaluated current intensity (0.15-2.5 mA) which span the range of previously established safety limits (Liebetanz et al., 2009, Rueger et al., 2012, Gellner et al., 2016). Ionized calcium-binding adapter molecule 1 (Iba1) activation was also examined as a more sensitive predictor of brain lesion. Brain tissue histology indicated lesions at a lower electrode current density (20.0 A/m^2) than previously reported. Therefore, we systematized our next experiments to critically evaluate this 20.0 A/m^2 limit while controlling the number and area of electrodes (10.6 mm^2 and 5.3 mm^2). Dissociating current intensity from electrode current density (e.g. same current intensity but different electrode current density), combined with high-resolution FEM computational models of current flow in rat, supported testing the hypothesis that brain current density, rather than simply electrode current intensity or electrode current density, predicts the propensity for lesions. This has important implications for how animal (rodent) models of tDCS, especially aimed at safety, are rationalized and applied to develop clinical guidelines.

2. Materials and Methods

2.1. 25.0 mm^2 Electrode Placement Surgery

Animals were anesthetized with isoflurane (Piramal Critical Care, Shop Med Vet, Mettawa, IL) using 5% induction and 2-3% maintenance. Animals were treated with standard pre- and

post-surgical care. The animal was placed into a stereotaxic apparatus and a caudo-rostral incision was made on top of the head, followed by a lateral incision was made at the shoulders. The periosteum was removed, the skull wiped clean, and a head electrode of 0.25 cm^2 (Valutrode, Axelgaard Manufacturing Co., Fallbrook, CA, 1.25-inch diameter electrode cut to 5mm × 5mm) with SignaGel (Parker Laboratories, Fairfield, NJ) was applied to the skull with the center of the electrode resting on the midline 2.5 mm caudal to Bregma (rostro-caudal: 0.0 mm to -5.0 mm). The insulated electrode wire was tunneled subcutaneously and exited the lateral incision made at shoulders. The electrode was held in place by a plastic head clamp which caught on the ridges of the skull (AFRL designed and produced) and two types of adhesives: C&B Metabond Adhesive Luting Cement (Parkell Inc., Edgewood, NY) was applied to the electrode and skull to create an initial bond, followed by acrylic cement (Stoelting, Co. Fisher Scientific, Pittsburg, PA) to bond the electrode to the clamp. Incisions were sutured closed around cement and wire. Animals recovered from surgery for at least 1 week prior to inclusion in experiments. Prior to stimulation, animals were randomly placed into six anodal tDCS treatment groups: 0.15 mA (n = 4), 0.3 mA (n = 4), 0.5 mA (n = 2), 1.0 mA (n = 4), 2.5 mA (n = 3), and sham stimulation (n = 3).

2.2. 10.6 mm^2 and 5.3 mm^2 Electrode Placement Surgery

Animals were prepared as described above and an electrode jacket with a surface area of 5.3 mm^2 (DIXI Medical, Besançon, France) was placed at -2.5 mm Bregma and 2.5 mm left of sagittal suture. The electrode jacket was secured with FUJI I glass ionomer (Dental Wholesale Direct, FL, USA), and a layer of dental cement was placed on top to further secure the electrode. Prior to stimulation, animals were assigned into 2 groups based on electrode placement: 1) a single 5.3 mm^2 electrode placed -2.5 mm Bregma and -2.5 mm left of the sagittal line (n=6), and 2) two 5.3 mm^2 electrodes placed at -2.5 mm Bregma and 2.5 mm from the midline bilaterally, for a total electrode surface area of 10.6 mm^2 (n = 5). Prior to stimulation, the animals were assigned into stimulation groups based on lesion results from the previous 25.0 mm^2 electrode experiment. The single electrode stimulation group was subdivided into groups based on current intensity: 2.0 mA (n = 1), 1.0 mA (n = 1), 0.75 mA (n = 1), 0.5 mA (n = 2), 0.05 mA (n = 1), and Sham (n = 1). The dual electrode group was also divided into subgroups based on current intensity: 2.0 mA (n = 1), 1.0 mA (n = 1), 0.5 mA (n = 1), 0.25 mA (n = 1), and sham (n = 1).

2.3. tDCS Application

2.3.1. 25.0 mm^2 Electrode Stimulation—Animals were anesthetized with isoflurane (Piramal Critical Care, Shop Med Vet, Mettawa, IL), using a 5% induction and 2-3% maintenance schedule. The reference electrode (8.04 cm^2, Valutrode, Axelgaard Manufacturing Co., Fallbrook, CA) was placed between the shoulders and SignaGel (Parker Laboratories, Fairfield, NJ) electrode gel was used as a conducting medium. A Petflex cohesive bandage (Andover, Shop Med Vet, Mettawa, IL) was wrapped around the midsection of the animal's torso to hold the reference electrode in place. tDCS was applied using a constant current stimulator (Magstim DC-stimulator, NeuroConn, Ilmenau, Germany) for 60 minutes in addition to a ramp-up/ramp-down period of 10 seconds. The sham animal group experienced the same experimental set-up as the treatment group, except

the constant current stimulator was off. The highest current the stimulator could provide (based on the current-delivery limitations of the stimulator) is 5.0 mA, which was intended to be the highest stimulation group. Throughout the stimulation at the highest intensity, however, the resistance levels of the circuit would increase and cause the stimulator to shut off. Following the automated shut down, the device was restarted at a current intensity 0.5 mA below the previous current intensity. The total duration remained at 60 minutes, but the current intensity varied during stimulation from 5.0 mA to 2.0 mA for the highest intensity group. The average intensity over the 60-minute duration for this group was approximately 2.5 mA and is referred to as the 2.5 mA condition throughout this manuscript.

2.3.2. 10.6 mm^2 and 5.3 mm^2 Electrode Stimulation—Animals were anesthetized with isoflurane (Piramal Critical Care, Shop Med Vet, Mettawa, IL), using a 5% induction and 2-3% maintenance schedule. The reference electrode (surface area: 1.3 cm^2; DIXI medical, Besançon, France) was placed on the chest and either saline or SignaGel was used as the electrolyte (Table 1). A Petflex bandage was wrapped around the animal's midsection to hold the reference electrode in place. SignaGel was placed into the electrode jacket, and tDCS was applied for 60 minutes using either a NeuroConn constant current stimulator (Jali Medical Inc., Waltham, MA, USA) or a Caputron constant current stimulator (Caputron Medical, New York, NY, USA) with a Silver Chloride (AgCl) electrode as the anode (Table 1). Note due to the smaller form factor, a change in material was required – none-the-less, the electrode current densities are below electrochemical injury thresholds (Merrill et al., 2005).

2.4. Histological Processing and Analysis

Immediately following the cessation of stimulation, animals were euthanized by Euthasol injection followed by exsanguination by cardiac perfusion using Phosphate Buffer Saline Solution (PBS) followed by 4% paraformaldehyde (PFA) to fix and preserve tissue. After perfusion, brains were removed and placed into 4% PFA solution for twenty-four hours and then transferred to 30% sucrose. Brains were kept in solution at 4° C until processed. A sliding microtome with a freezing plate (Leica SM2010R) was used for serial collection of 16-micron thick coronal sections and were placed into a cryoprotectant solution and stored at -20 ° C until further processing.

2.4.1. Tissue Staining: H&E, Iba1—Tissue sections were removed from the cryoprotectant solution, washed for 5 minutes in 1× Phosphate Buffered Saline (PBS) 5 times and mounted onto slides using a 0.1× Phosphate Buffer Solution (PB) with 5% gelatin. Tissue sections were stained with hematoxylin and eosin (H&E). For staining of the ionizing calcium-binding adaptor molecule 1 (Iba1) protein, a set of six sections from each animal was removed from the cryoprotectant solution and washed 5 times for 5 minutes each in 1× PBS. Endogenous peroxidase was blocked (10% methanol, 3% H_2O_2 in PBS) for 15 minutes and slices were then transferred into blocking buffer (PBS solution with 5% Triton-X100 and 2% goat serum) for one hour. Sections were then incubated with the rabbit polyclonal anti-ionized calcium binding adapter molecule antibody (Iba1, Wako Chemicals USA, Inc., Richmond, VA, USA, 1: 3,000 dilution) in blocking buffer solution refrigerated overnight on a Thermo Scientific MaxQ 4000 shaker at 75 rpm. The sections were washed and incubated

for 2 hours at room temperature with the biotinylated secondary goat anti-rabbit antibody (Vector Laboratories, Burlingame, CA at 1: 3,000 dilution) in blocking buffer solution for 2 hours. Sections were washed again and incubated for 1 hour with Vectastain Elite ABC kit (Vector Laboratories, Burlingame, CA, USA) for enzyme conjugation. Finally, sections were stained using 0.05% diaminobenzidine and 0.5% nickel ammonium sulfate and 0.03% H_2O_2. Tissue sections were then mounted onto slides and allowed to dry at room temperature overnight. Subsequently, sections were counterstained with H&E as previously described for co-localization of lesion and microglial cells. DPX mountant (Sigma, Saint Louis, MO, USA) was used as a coverslip adhesive.

2.4.2. Image Analysis—All images were collected using an Olympus BX63 microscope with a Q100 Blue Camera designed for CellSens Dimension Software. Researchers quantifying lesion were blinded to treatment groups throughout tissue processing, image collection and analysis. CellSens Dimension software was used to determine and quantify the area of lesion damage, and a Rat Brain Atlas (Paxinos et al., 2007) was used to order sections rostral to caudal according to their distance from Bregma (mm). Lesion was visually identified by parenchymal discoloration and striation in addition to visible gross cellular alterations such as edema, karyolysis and apparent cell loss in the outermost cortical layer. Percent area of Iba-1 positive staining was quantified in cortical samples per electrode placement group using 10× magnification. The software used hue, saturation and intensity (HSI) to segment the image fields. Thresholds for object segmentation were established with images of high and low levels of staining to identify positive staining over any background level. These limits were held constant for the analysis of every section in the study. Cell body area and roundness outcomes were measured using the count and measure component from CellSens Dimension software. Briefly, cell bodies were outlined from a sampled cortical area from each section. Placement of the region of interest analyzed was kept constant at all sections and positioned in areas where current-induced lesions were mostly likely to occur. Cell body area (in μm^2) and roundness were measured, where perfectly round objects are scored as 1.

2.5. Computational Modeling

To determine the effect of various current densities on brain lesion, a state-of-the-art model was constructed from a MRI (7.0 Tesla 70/30 Bruker Biospec) and micro-CT scan (Siemens Inveon) of a female rat (Song et al., 2015).

2.5.1. MRI Data Collection and Segmentation—MRI resolution was 0.282-mm, as previously mentioned (Song et al., 2015). The scans were segmented into 9 tissues: skin, skull, cerebral spinal fluid (CSF), air, gray matter, white matter, hippocampus, cerebellum, and spinal cord. A Rat Brain Atlas (Paxinos et al., 2007) was used to identify the hippocampal region of the brain, and the remaining brain regions were appropriately grouped as either gray or white matter.

Manual segmentation was used to generate an initial segmentation of scalp, skin, CSF, air, gray matter, white matter, hippocampus, cerebellum, and spinal cord. Tissue continuity was verified after segmentation by extensively reviewing the data, and further manual

adjustments were made to guarantee continuity and improve the segmentation accuracy to closely match the tissue masks to the real anatomy of the rodent using ScanIP 7.0 (Simpleware Ltd, Exeter, UK).

2.5.2. Modeling of tDCS—The three *in vivo* electrode placement protocols described above were modeled in SolidWorks (Dassault Systemes Corp. Waltham, MA) and imported into ScanIP for meshing. Three montages were modeled: 1) 5mm × 5mm anode (surface area: 23.21 mm^2) placed on the skull at 0.0 mm Bregma; 2) a single 5.3 mm^2 electrode (surface area: 4.84 mm^2) placed on the skull at – 2.5 mm Bregma and 2.5 mm left of the sagittal suture; and 3) two 5.3 mm^2 electrodes (total surface area: 9.68 mm^2) placed on the skull at -2.5 mm Bregma and 2.5 mm bilaterally from the sagittal suture. The first montage used an 8.04 cm^2 cathode placed between the shoulder blades, while the last two used a 1.3 cm^2 cathode placed on the chest. An adaptive tetrahedral meshing algorithm was used in ScanIP to generate meshes of 8×10^6 quadratic elements.

FEM models were created in COMSOL Multiphysics 4.3 (COMSOL, Inc., Burlington, MA) using the meshes mentioned above. Models were created using electrostatic volume conductor physics with material conductivities defined as follows (in S/m): skin, 0.465; skull, 0.01; CSF, 1.65; air, $1e^{-15}$; spinal cord, 0.126; gray matter, 0.276; white matter, 0.126; hippocampus, 0.126; cerebellum, 0.276; dental cement, $1e^{-15}$; electrode jacket, $1e^{-15}$; saline, 1.4; and electrode, $5.99e^7$. These conductivity values were taken from a combination of in vitro and in vivo measurements (Datta et al., 2009b, Minhas et al., 2010). Current boundaries were applied to simulate direct current stimulation, and internal boundaries between tissues were assigned the continuity condition ($n * (J_1 – J_2) = 0$), and the Laplace equation ($\nabla * (\sigma \nabla V) = 0$) was solved. The surface of the cathode was grounded ($V = 0$) while the surface of the anodes for the three stimulation montages had a current density at which lesion first appeared *in vivo*: 1) 20.0 A/m^2; 2) 23.5 A/m^2; and 3) 94.2 A/m^2. All other exterior surfaces were electrically insulated, and brain current density data from the medial cortex between the most superficial regions of the corpus callosum were collected and averaged for analysis. High-resolution models predicted the concentration and distribution of brain current density for each *in vivo* stimulation group using the three electrode montages. Brain current density is shown for representative coronal sections in false-color, where brain current density values less than 0.34184 A/m^2 are represented in blue, and brain current density values greater than 7.04619 A/m^2 are presented in dark red. The maximum threshold was determined by preliminary analysis corresponding the first appearance of lesion *in vivo*.

2.6. Statistical Analysis

Statistical analysis was performed using SigmaPlot (SigmaPlot 11.0, San Jose, CA) for only the 25.0 mm^2 electrode group unless otherwise noted. One-way analysis of variance (ANOVA) was used for group comparisons followed by Tukey post hoc test. Statistical significance was established with $p<0.05$ for all tests. Two-way ANOVA, three-way ANOVA, and one tailed t-tests were also used and are distinguished in the text.

3. Results

3.1. Brain lesion from anodal tDCS

This study aimed to compare the effects of electrode size (25.0 mm^2, 10.6 mm^2, and 5.3 mm^2) on brain lesion at various electrode current densities using anodal tDCS (Table 1). Computational modeling was used to further analyze and compare histological brain lesion (Figure 1). No apparent lesions were present using the 25.0 mm^2 electrode in the sham, 0.15 mA, or 0.3 mA stimulation groups, whereas the 0.5 mA, 1.0 mA, and 2.5 mA stimulation groups had increasingly larger areas of parenchymal discoloration and cellular alterations. Tissue sections from the 0.5 mA stimulation group showed small lesions at the medial cortex on the outer cortical surface (Figure 1A). Compared to tissue sections obtained from the 0.5 mA group, morphological changes in the 1.0 mA group were more extensive, penetrating deeper into the cortex and expanding laterally across the outer cortical layer. Lesion in the 2.5 mA group was the most extensive compared to the other stimulation groups (Figure 1A).

FEM analysis predicts the greatest brain current density (above 7.04619 A/m^2) will occur in the medial cortex and in deeper and more lateral brain regions at higher applied currents, such as the corpus callosum, hippocampus, and thalamus (Figure 1A). Histologically, however, the alterations in morphology from each stimulation group were only observed in cortical brain regions.

Histological lesion was not present in the Sham group using the dual electrode design (total electrode surface area: 10.6 mm^2), but lesion was present on the medial cortex at current intensities at and above 0.25 mA (Figure 1B). Lesion was more extensive for higher stimulation groups, spreading laterally and penetrating deeper into the tissue. Brain current density analysis of the dual electrode design at 0.25 mA showed brain current density was greatest in the superficial cortical regions. At 0.5 mA, brain current density above 0.34184 A/m^2 was present in the entire medial cortex as well as the medial corpus callosum at 1.0 mA (Figure 1B). Histological observation of tissue damage was only noted in the superficial cortical regions.

The single 5.3 mm^2 electrode design did not produce histological lesions in the Sham or 0.043 mA stimulation groups, but morphological changes were detected at 0.5 mA, 0.75 mA, 1 mA, and 2 mA (Figure 1C). The morphological changes began in the motor cortical region at 0.5 mA, and spread laterally across the outer cortex at higher stimulation groups; there was bilateral lesion present at 2.0 mA (figure 1C; bottom). The greatest brain current densities (above 7.04619 A/m^2) for the single 5.3 A/m^2 electrode occurred unilaterally in the cortex and corpus callosum with an applied current of 0.5 mA (Figure 1C) and spread bilaterally at greater applied current intensities. Brain current densities above 0.34184 A/m^2 were bilaterally present in the cortex and unilaterally in the CA1 region of the hippocampus using 1.0 mA. At 2.0 mA, brain current densities above 7.04619 A/m^2 were seen bilaterally in the corpus callosum, hippocampus, and superficial thalamus (Figure 1C).

Total brain lesion was quantified by measuring and averaging the area of parenchymal alterations for each stimulation group (Figure 2). Using a 25.0 mm^2 electrode, brain damage was present at 20.0 A/m^2 (average area = 0.50 $mm^2 \pm$ 0.304), 40 A/m^2 (average area = 15.77

mm^2± 2.365), and 100 A/m^2 (average area = 40.92 mm^2± 0.937). Animals receiving 40 A/m^2 and 100 A/m^2 had a significantly greater lesion area compared to all other groups (One-way ANOVA: $F(5) = 178.8$, $p<0.001$, for both groups). No statistically significant differences occurred between the sham, 0.15 A/m^2, 0.3 A/m^2, or 0.5 A/m^2 groups (Figure 2A). Cortical lesion at similar electrode current densities using different electrode sizes was evaluated and appears to be positively correlated with both electrode size and electrode current density (Figure 2B). Across the three electrode groups, lesion was significantly different at an electrode current density of 100.0 A/m^2 (One-way ANOVA: $F(1) = 519.1$, $p < 0.001$: 25.0 mm^2 = 40.92 mm^2± 0.937, 10.6 mm^2 = 15.77mm^2± 2.365, 5.3 mm^2 = 0.50 mm^2± 0.304).

Brain lesion area was quantified in coronal slices based on distance from Bregma (Figure 3). Lesion area in tissue sections (Figure 3A) were statistically different (two-way ANOVA: $F(23) =18.543$, $p<0.001$) in tissue sections that were between +2.0 mm and -6.5 mm from Bregma using a 25.0 mm^2 electrode (black lines above figure 3A). The lesion area at each location from Bregma was significantly different when compared between: 1) 2.5 mA and 0.5 mA, from +2.0 mm to -6.5 mm Bregma (two-way ANOVA; $p<0.02$); 2) 2.5 mA and 1.0 mA from +0.5 mm to -6.5 mm Bregma (two-way ANOVA; $p<0.02$); and 3) 1.0 mA and 0.5 mA from +2.0 mm to -4.5 mm (two-way ANOVA; $p<0.05$). Lesion area differences based on distance from Bregma were also present for the 10.6 mm^2 (Figure 3B) and 5.3 mm^2 (Figure 3C) electrodes. Using FEM rodent models to predict the average brain current density in coronal sections at 0.5 mm increments from +5 mm Bregma to -6.5 mm Bregma, a larger electrode corresponds to a greater average brain current density across all coronal sections at approximately 100 A/m^2. (Figure 3D).

We compared the reliability of electrode current density and average brain current density from models for predicting brain lesion area across the three electrode sizes (Figure 4). For each electrode, lesion area increased linearly ($R2=0.2442$) with electrode current density, but the electrode's sensitivity (slope) to lesion varied (Figure 4A). At an electrode current density of 100 A/m^2, the lesion area for the 5.3 mm^2, 10.6 mm^2, and 25.0 mm^2 electrodes are 6.1 mm^2, 18.9 mm^2, and 40.9 mm^2, respectively. Lesion area also increased linearly with brain current density ($R^2=0.8139$) and sensitivity to lesion development was similar across the three electrode sizes (Figure 4B).

3.2. Iba1 immunoreactivity

To investigate whether tDCS affected inflammation in the brain, tissue sections were stained with an antibody against Iba1, a protein that is present in macrophages and microglia and upregulated when in their active state (Hanisch et al., 2007). There were no differences in the percentage of positive Iba1 staining in the cortical areas immediately below the electrode ($p=0.50$, data not shown). However, microglial morphology trended towards a more activated phenotype, with enlarged cell bodies and thickened processes, in stimulation groups that produced lesion (0.5 mA and higher; Figure 5). No statistical differences occurred in Iba1 positive cell body surface area ($p=0.61$, figure 5E), but there was a statistical significance between current intensity and cell body roundness. At 1.0 mA,

microglial cell bodies were significantly more rounded compared to all other groups (p=0.02, figure 5F).

4. Discussion

We detected cortical lesions during anodal stimulation using an electrode current density of 20.0 A/m^2, which is well below the commonly referenced cathodal electrode current density threshold of 142.9 A/m^2 (Liebetanz et al., 2009). Histological analysis did not reveal any lesion at or below 0.3 mA using a 25.0 mm^2 electrode, corresponding to an electrode current density of 12 A/m^2. This was the greatest applied current intensity that could be administered for 60 minutes without evidence of tissue damage using the 25.0 mm^2 electrode.

The lesions from our study expanded laterally and penetrated deeper into the tissue as the electrode current density was increased (Figure 1). However, the lesion induced from the Liebetanz study appeared to penetrate more deeply and less laterally with increasing electrode current densities, which may reflect differences in electrode montage (including position of the return electrode) or polarity specific mechanisms of injury (anodal vs. cathodal tDCS). Once correcting for average brain current density, our finding of comparable dose response across changes in electrode material, shape, and number are consistent with brain current flow, rather than superficial electrochemistry, causing injury.

Microglial cells have been shown to increase after sub-lesion tDCS when assessed by measuring Iba1+ cells three days after stimulation (Rueger et al., 2012), possibly providing evidence of a more sensitive marker of tDCS related injury than lesion. Our exploratory analysis of microglia and macrophage immunoreactivity showed no significant changes in the percentage of immunoreactive cells present in the medial cortex following a 60-minute stimulation (Figure 5), but higher current densities were likely already shifting the microglial phenotype from its resting to active state. Despite the untimely approach for microglial analysis, our histological data did show an increase in cell body roundness at 1.0 mA immediately after tDCS (figure 5F), suggesting either tDCS or the induction of lesion shifted microglia to its active. This study was not able to make a distinction histologically due to our flawed approach, but it has been shown microglial changes associated with neuroinflammation can occur at approximately 31.8 A/m^2 using anodal tDCS (Gellner et al., 2016).

Although **investigation of multiple** tDCS parameters is possible utilizing a rodent model, there are translational limitations. One of those limitations is the ability to easily approximate and translate tDCS dosages between small, 300-500 g animals and large 70 kg humans. However, FEM analysis of *in vivo* rodent experiments has attempted to translate rodent lesion studies to determine a lesion threshold in humans by developing a scaling factor, with the most conservative prediction of injury from rodent FEM models occurring in humans at 6.3 A/m^2 (Bikson et al., 2016). Understanding and translating minimum lesion thresholds in rodents could allow a greater range of safe stimulation protocols for human applications, potentially enhancing benefits already seen in human tDCS. Our data show damage can occur at a level of 20.0 A/m^2 (figure 4). However, this threshold is 10-fold

higher than the typical electrode current density of 0.28 – 2.0 A/m^2 utilized in human studies (Poreisz et al., 2007, McKinley et al., 2013). Moreover, our model is hypersensitive compared to the clinical case where electrodes are placed on the skin (not epicranial) and the distance between the electrode and brain is significantly higher. Taken together with our consideration of appropriate safety metrics (above), our threshold for electrode current density in rat models may be conservatively considered (with a safety factor) applicable to the human case.

5. Conclusions

Our anodal animal tDCS study shows tissue damage can occur at 20.0 A/m^2, which is below the often referenced damage threshold of 142.9 A/m^2 using cathodal tDCS (Liebetanz et al., 2009). In considering the relevance of animal studies to human safety guidelines, consideration should also be given to the role of electrode size, location, and brain region of interest. Consistent with prior studies, our data does not suggest current clinical tDCS are injurious.

Acknowledgments

This work could not have been completed without the help of the following individuals: Wilson C. Tucker, Naomi Bechmann, Raquel Moore, Saline Hughes, Kimberly A.K. Carhuatanta, Melanie Chin, Justin Stafford, Victoria Dreshem, Dick Godfrey and Andrew Jimenez. This work was supported by the Air Force Office of Scientific Research.

Funding: This work was supported by the Air Force Office of Scientific Research (Grant 13RH14COR, 16RHCOR362), NIH (Award# 5R03EB017410-02, 5R21EB017510-02, 5R01MH092926-05) and DoD (Award# FA9550-13-1-0073)

References

Agnew WF, McCreery DB. Considerations for Safety in the Use of Extracranial Stimulation for Motor Evoked Potentials. Neurosurgery. 1987; 20:143–7. [PubMed: 3808255]

Baker JM, Rorden C, Fridriksson J. Using transcranial Direct-current Stimulation to Treat Stroke Patients with Aphasia. Stroke. 2010; 41:1229–36. [PubMed: 20395612]

Bikson M, Datta A, Elwassif M. Establishing Safety Limits for transcranial Direct Current Stimulation. Clin Neurophysiol. 2009; 120:1033–4. [PubMed: 19394269]

Bikson M, Grossman P, Thomas C, Zannou AL, Jiang J, Adnan T, et al. Safety of Transcranial Direct Current Stimulation: Evidence Based Update 2016. Brain Stimul. 2016

Bikson M, Inoue M, Akiyama H, Deans JK, Fox JE, Miyakawa H, et al. Effects of uniform extracellular DC electric fields on excitability in rat hippocampal slices in vitro. J Physiol. 2004; 557:175–90. [PubMed: 14978199]

Brunoni AR, Boggio PS, Ferrucci R, Priori A, Fregni F. Transcranial direct current stimulation: challenges, opportunities, and impact on psychiatry and neurorehabilitation. Front Psychiatry. 2013; 4:19. [PubMed: 23544030]

Brunoni AR, Ferrucci R, Bortolomasi M, Vergari M, Tadini L, Boggio PS, et al. Transcranial direct current stimulation (tDCS) in unipolar vs. bipolar depressive disorder. Prog Neuropsychopharmacol Biol Psychiatry. 2011; 35:96–101. [PubMed: 20854868]

Brunoni AR, Nitsche MA, Bolognini N, Bikson M, Wagner T, Merabet L, et al. Clinical Research with transcranial Direct Current Stimulation (tDCS): Challenges and Future Directions. Brain Stimul. 2012; 5:175–95. [PubMed: 22037126]

Brunoni AR, Vanderhasselt MA. Working memory improvement with non-invasive brain stimulation of the dorsolateral prefrontal cortex: a systematic review and meta-analysis. Brain Cogn. 2014; 86:1–9. [PubMed: 24514153]

Castillo-Saavedra L, Gebodh N, Bikson M, Diaz-Cruz C, Brandao R, Coutinho L, et al. Clinically Effective Treatment of Fibromyalgia Pain With High-Definition Transcranial Direct Current Stimulation: Phase II Open-Label Dose Optimization. J Pain. 2016; 17:14–26. [PubMed: 26456677]

Crespo-Garcia S, Reichhart N, Hernandez-Matas C, Zabulis X, Kociok N, Brockmann C, et al. In vivo analysis of the time and spatial activation pattern of microglia in the retina following laser-induced choroidal neovascularization. Exp Eye Res. 2015; 139:13–21. [PubMed: 26213305]

Dasilva AF, Mendonca ME, Zaghi S, Lopes M, Dossantos MF, Spierings EL, et al. tDCS-induced analgesia and electrical fields in pain-related neural networks in chronic migraine. Headache. 2012; 52:1283–95. [PubMed: 22512348]

Datta A, Bansal V, Diaz J, Patel J, Reato D, Bikson M. Gyri-precise head model of transcranial direct current stimulation: improved spatial focality using a ring electrode versus conventional rectangular pad. Brain Stimul. 2009a; 2:201–7. 7 e1. [PubMed: 20648973]

Datta A, Elwassif M, Bikson M. Bio-heat Transfer Model of tDCS-Comparison of Conventional Pad versus Ring Electrode. Conf Proc IEEE Eng Med Biol Soc. 2009b:670–3. [PubMed: 19964238]

Datta A, Truong D, Minhas P, Parra LC, Bikson M. Inter-Individual Variation during Transcranial Direct Current Stimulation and Normalization of Dose Using MRI-Derived Computational Models. Front Psychiatry. 2012; 3:91. [PubMed: 23097644]

Davalos D, Grutzendler J, Yang G, Kim JV, Zuo Y, Jung S, et al. ATP mediates rapid microglial response to local brain injury in vivo. Nat Neurosci. 2005; 8:752–8. [PubMed: 15895084]

Edwards DJ, Krebs HI, Rykman A, Zipse J, Thickbroom GW, Mastaglia FL, et al. Raised corticomotor excitability of M1 forearm area following anodal tDCS is sustained during robotic wrist therapy in chronic stroke. Restor Neurol Neurosci. 2009; 27:199–207. [PubMed: 19531875]

Fregni F, Boggio PS, Lima MC, Ferreira MJ, Wagner T, Rigonatti SP, et al. A sham-controlled, phase II trial of transcranial direct current stimulation for the treatment of central pain in traumatic spinal cord injury. Pain. 2006; 122:197–209. [PubMed: 16564618]

Fridriksson J, Richardson JD, Baker JM, Rorden C. Transcranial direct current stimulation improves naming reaction time in fluent aphasia: a double-blind, sham-controlled study. Stroke. 2011; 42:819–21. [PubMed: 21233468]

Galletta EE, Cancelli A, Cottone C, Simonelli I, Tecchio F, Bikson M, et al. Use of Computational Modeling to Inform tDCS Electrode Montages for the Promotion of Language Recovery in Post-stroke Aphasia. Brain Stimul. 2015

Gbadeyan O, Steinhauser M, McMahon K, Meinzer M. Safety, Tolerability, Blinding Efficacy and Behavioural Effects of a Novel MRI-Compatible, High-Definition tDCS Set-Up. Brain Stimul. 2016; 9:545–52. [PubMed: 27108392]

Gellner AK, Reis J, Fritsch B. Glia: A Neglected Player in Non-invasive Direct Current Brain Stimulation. Front Cell Neurosci. 2016; 10:188. [PubMed: 27551261]

Hanisch UK, Kettenmann H. Microglia: active sensor and versatile effector cells in the normal and pathologic brain. Nat Neurosci. 2007; 10:1387–94. [PubMed: 17965659]

Holland R, Crinion J. Can tDCS enhance treatment of aphasia after stroke? Aphasiology. 2012; 26:1169–91. [PubMed: 23060684]

Jackson MP, Rahman A, Lafon B, Kronberg G, Ling D, Parra LC, et al. Animal models of transcranial direct current stimulation: Methods and mechanisms. Clin Neurophysiol. 2016; 127:3425–54. [PubMed: 27693941]

Kabakov AY, Muller PA, Pascual-Leone A, Jensen FE, Rotenberg A. Contribution of axonal orientation to pathway-dependent modulation of excitatory transmission by direct current stimulation in isolated rat hippocampus. J Neurophysiol. 2012; 107:1881–9. [PubMed: 22219028]

Kasschau M, Sherman K, Haider L, Frontario A, Shaw M, Datta A, et al. A Protocol for the Use of Remotely-Supervised Transcranial Direct Current Stimulation (tDCS) in Multiple Sclerosis (MS). J Vis Exp. 2015:e53542. [PubMed: 26780383]

Kronberg G, Bridi M, Abel T, Bikson M, Parra LC. Direct Current Stimulation Modulates LTP and LTD: Activity Dependence and Dendritic Effects. Brain Stimul. 2017; 10:51–8. [PubMed: 28104085]

Liebetanz D, Koch R, Mayenfels S, Konig F, Paulus W, Nitsche MA. Safety Limits of Cathodal transcranial Direct Current Stimulation in Rats. Clin Neurophysiol. 2009; 120:1161–7. [PubMed: 19403329]

Loo CK, Alonzo A, Martin D, Mitchell PB, Galvez V, Sachdev P. Transcranial direct current stimulation for depression: 3-week, randomised, sham-controlled trial. Br J Psychiatry. 2012; 200:52–9. [PubMed: 22215866]

Marquez-Ruiz J, Leal-Campanario R, Sanchez-Campusano R, Molee-Ardekani B, Wendling F, Miranda PC, et al. Transcranial direct-current stimulation modulates synaptic mechanisms involved in associative learning in behaving rabbits. Proc Natl Acad Sci U S A. 2012; 109:6710–5. [PubMed: 22493252]

McCreery DB, Agnew WF, Yuen TG, Bullara L. Charge density and charge per phase as cofactors in neural injury induced by electrical stimulation. IEEE Trans Biomed Eng. 1990; 37:996–1001. [PubMed: 2249872]

McKinley RA, McIntire L, Bridges N, Goodyear C, Bangera NB, Weisend MP. Acceleration of image analyst training with transcranial direct current stimulation. Behav Neurosci. 2013; 127:936–46. [PubMed: 24341718]

Merrill DR, Bikson M, Jefferys JG. Electrical stimulation of excitable tissue: design of efficacious and safe protocols. J Neurosci Methods. 2005; 141:171–98. [PubMed: 15661300]

Minhas P, Bansal V, Patel J, Ho JS, Diaz J, Datta A, et al. Electrodes for high-definition transcutaneous DC stimulation for applications in drug delivery and electrotherapy, including tDCS. J Neurosci Methods. 2010; 190:188–97. [PubMed: 20488204]

Miranda PC, Faria P, Hallett M. What does the ratio of injected current to electrode area tell us about current density in the brain during tDCS? Clin Neurophysiol. 2009; 120:1183–7. [PubMed: 19423386]

Nitsche MA, Doemkes S, Karakose T, Antal A, Liebetanz D, Lang N, et al. Shaping the effects of transcranial direct current stimulation of the human motor cortex. J Neurophysiol. 2007; 97:3109–17. [PubMed: 17251360]

Nitsche MA, Nitsche MS, Klein CC, Tergau F, Rothwell JC, Paulus W. Level of action of cathodal DC polarisation induced inhibition of the human motor cortex. Clinical Neurophysiology. 2003; 114:600–4. [PubMed: 12686268]

Nitsche MA, Paulus W. Excitability Changes induced in the Human Motor Cortex by Weak transcranial Direct Current Stimulation. J Physiol. 2000; 527(3):633–9. [PubMed: 10990547]

Nitsche MA, Paulus W. Vascular safety of brain plasticity induction via transcranial direct currents. Neurology. 2015; 84:556–7. [PubMed: 25576637]

Palm U, Segmiller FM, Epple AN, Freisleder FJ, Koutsouleris N, Schulte-Korne G, et al. Transcranial direct current stimulation in children and adolescents: a comprehensive review. J Neural Transm (Vienna). 2016

Paxinos, G., Watson, C. The Rat Brain in Stereotaxic Coordinates. 6. Elsevier Science; 2007.

Peterchev AV, Wagner TA, Miranda PC, Nitsche MA, Paulus W, Lisanby SH, et al. Fundamentals of transcranial electric and magnetic stimulation dose: definition, selection, and reporting practices. Brain Stimul. 2012; 5:435–53. [PubMed: 22305345]

Pikhovych A, Stolberg NP, Jessica Flitsch L, Walter HL, Graf R, Fink GR, et al. Transcranial Direct Current Stimulation Modulates Neurogenesis and Microglia Activation in the Mouse Brain. Stem Cells Int. 2016a; 2016:2715196. [PubMed: 27403166]

Pikhovych A, Walter HL, Mahabir E, Fink GR, Graf R, Schroeter M, et al. Transcranial direct current stimulation in the male mouse to promote recovery after stroke. Lab Anim. 2016b; 50:212–6. [PubMed: 26442519]

Podda MV, Cocco S, Mastrodonato A, Fusco S, Leone L, Barbati SA, et al. Anodal transcranial direct current stimulation boosts synaptic plasticity and memory in mice via epigenetic regulation of Bdnf expression. Sci Rep. 2016; 6:22180. [PubMed: 26908001]

Poreisz C, Boros K, Antal A, Paulus W. Safety aspects of transcranial direct current stimulation concerning healthy subjects and patients. Brain Res Bull. 2007; 72:208–14. [PubMed: 17452283]

Rahman A, Reato D, Arlotti M, Gasca F, Datta A, Parra LC, et al. Cellular Effects of Acute Direct Current Stimulation: Somatic and Synaptic Terminal Effects. J Physiol. 2013; 591:2563–78. [PubMed: 23478132]

Rohan JG, Carhuatanta KA, McInturf SM, Miklasevich MK, Jankord R. Modulating Hippocampal Plasticity with In Vivo Brain Stimulation. J Neurosci. 2015; 35:12824–32. [PubMed: 26377469]

Rueger MA, Keuters MH, Walberer M, Braun R, Klein R, Sparing R, et al. Multi-session transcranial direct current stimulation (tDCS) elicits inflammatory and regenerative processes in the rat brain. PLoS One. 2012; 7:e43776. [PubMed: 22928032]

Saturnino GB, Antunes A, Thielscher A. On the Importance of Electrode Parameters for Shaping Electric Field Patterns Generated by tDCS. Neuroimage. 2015; 120:25–35. [PubMed: 26142274]

Song W, Truong DQ, Bikson M, Martin JH. Transspinal direct current stimulation immediately modifies motor cortex sensorimotor maps. J Neurophysiol. 2015; 113:2801–11. [PubMed: 25673738]

Stence N, Waite M, Dailey M. Dynamics of microglial activation: A confocal time-lapse analysis in hippocampal slices. Glia. 2001; 33:256–66. [PubMed: 11241743]

Tanga FY, Raghavendra V, DeLeo JA. Quantitative real-time RT-PCR assessment of spinal microglial and astrocytic activation markers in a rat model of neuropathic pain. Neurochem Int. 2004; 45:397–407. [PubMed: 15145554]

Truong DQ, Magerowski G, Blackburn GL, Bikson M, Alonso-Alonso M. Computational Modeling of transcranial Direct Current Stimulation (tDCS) in Obesity: Impact of Head Fat and Dose Guidelines. Neuroimage Clin. 2013; 2:759–66. [PubMed: 24159560]

Wachter D, Wrede A, Schulz-Schaeffer W, Taghizadeh-Waghefi A, Nitsche MA, Kutschenko A, et al. Transcranial direct current stimulation induces polarity-specific changes of cortical blood perfusion in the rat. Exp Neurol. 2011; 227:322–7. [PubMed: 21147105]

Wong CS, Jow GM, Kaizaki A, Fan LW, Tien LT. Melatonin ameliorates brain injury induced by systemic lipopolysaccharide in neonatal rats. Neuroscience. 2014; 267:147–56. [PubMed: 24613717]

Woods AJ, Antal A, Bikson M, Boggio PS, Brunoni AR, Celnik P, et al. A technical guide to tDCS, and related non-invasive brain stimulation tools. Clin Neurophysiol. 2016; 127:1031–48. [PubMed: 26652115]

Yuen TG, Agnew WF, Bullara LA, Jacques S, McCreery DB. Histological evaluation of neural damage from electrical stimulation: considerations for the selection of parameters for clinical application. Neurosurgery. 1981; 9:292–9. [PubMed: 7301072]

Highlights

1. Anodal tDCS can induce brain lesion using rodent models at an electrode current density of 20.0 A/m^2 (2.0 mA/cm^2) - significantly lower than previous estimates.
2. First rodent experiments with varied electrode montages and FEM analysis suggest average brain current density, rather than electrode current density, as a better predictor of brain lesion.
3. Translationally meaningfully animal models of tDCS safety must be carefully rationalized.

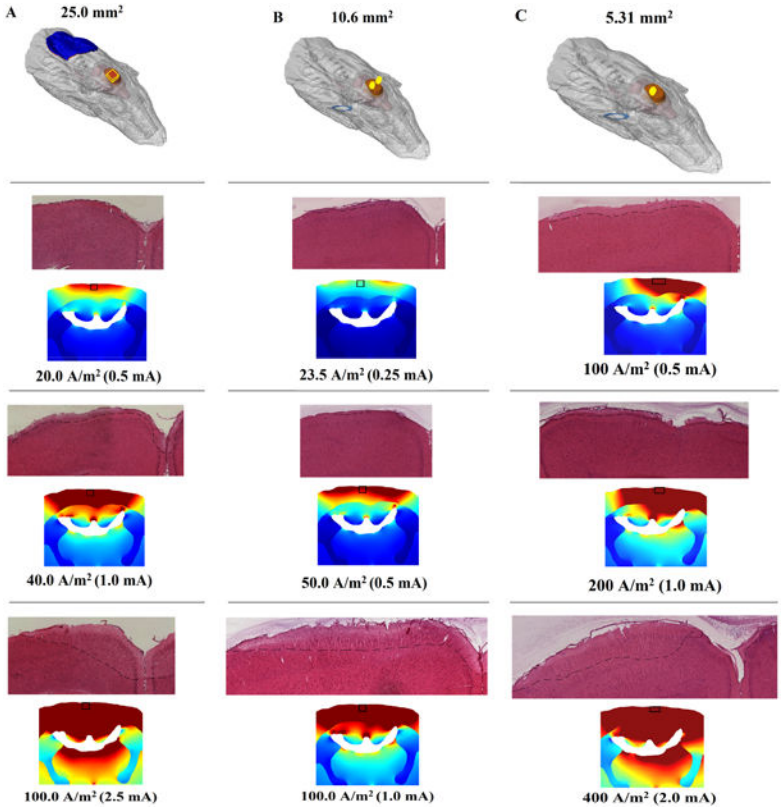

Figure 1.

Micrograph representation (4×) of both H&E stained coronal sections from tDCS-induced brain lesion and current distribution at or near -2.5 mm Bregma. Increasing tDCS current increases brain lesion in the rat as well as computationally regardless of electrode size (A, B, C). The anode (red) was placed on the skull, while the cathode (blue) was placed on either the back or chest. **A**. Using a 25.0 mm^2 electrode, a minimum electrode current density of approximately 20.0 A/m^2 induces cortical lesion beginning in the medial superficial cortex, which spreads laterally and penetrates into the cortex as the electrode current density is doubled. The 2.5 mA stimulation group showed e lesion was greater laterally and penetrated further into the cortex compared to the lower stimulation groups. **B**. Cortical damage begins to appear in the medial superficial cortex with a 0.25 mA (electrode current density: 23.5 A/m^2) stimulation using a 10.6 mm^2 electrode. The lesion area is also greater when the current intensity is increased. **C**. Using a 5.3 mm^2 electrode, lesion began to appear at 0.5 mA (electrode current density: 94.2 A/m^2) beginning in the motor cortex and expanded as the current intensity was increased.

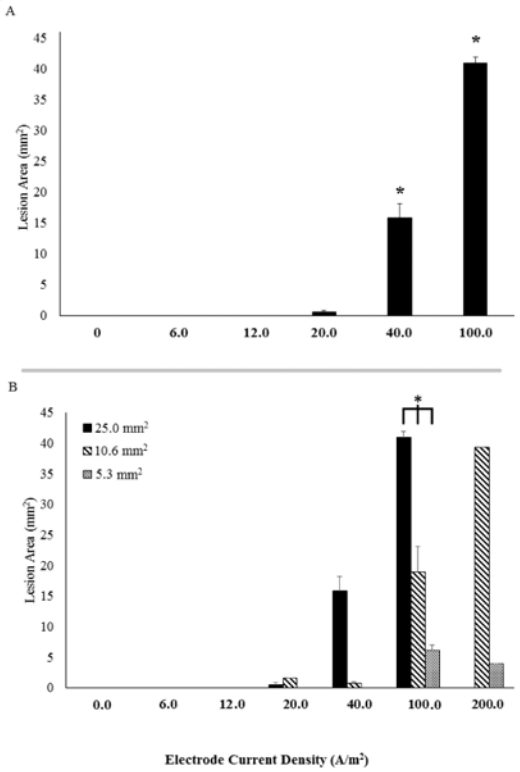

Figure 2.

Average lesion area evaluated by electrode current density. **A.** Lesion area was quantified in H&E stained sections obtained from animals at all current intensities after tDCS with a 25.0 mm^2 electrode implanted on the skull. No lesions were observed at currents less than 0.5 mA, but were detected with currents of 0.5 mA and greater. * indicates significant differences from all other stimulation groups ($p<0.001$). **B.** All electrode sizes are evaluated for average lesion area and separated by electrode current density. Delivering anodal tDCS at a higher electrode current density appears to show lesion area is dependent on the size of the electrode, with a larger electrode producing a larger lesion. * indicates a significant difference between electrode sizes at 100 A/m^2.

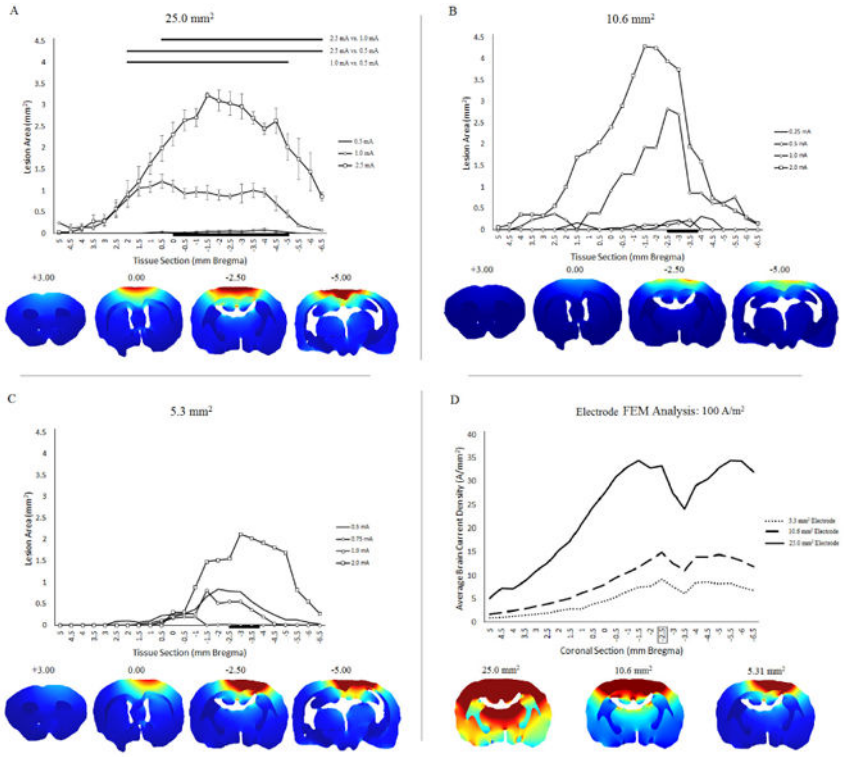

Figure 3.

Averaged lesion area by brain tissue section and electrode size according to its distance from Bregma. The average brain lesion was quantified in 0.5 mm increments, with positive numbers indicating the distance rostral from Bregma, and negative numbers indicating the distance caudal from Bregma. **A, B, C.** Local differences in cortical lesion for the 25.0 mm^2 (A), 10.6 mm^2 (B), and 5.3 mm^2 (C) electrodes, separated by the stimulation group. FEM images show rostro-caudal changes in brain current density at representative coronal sections. The black line at the bottom of the figure indicates the location of the electrode. Significant differences between current intensity and the average lesion produced at specific locations from Bregma are indicated at the top of (A). **D.** FEM analysis of brain current density in the medial cortex corresponding with in vivo tissue sections (mm Bregma). The box around -2.5 mm Bregma indicates the location of the FEM images below the figure.

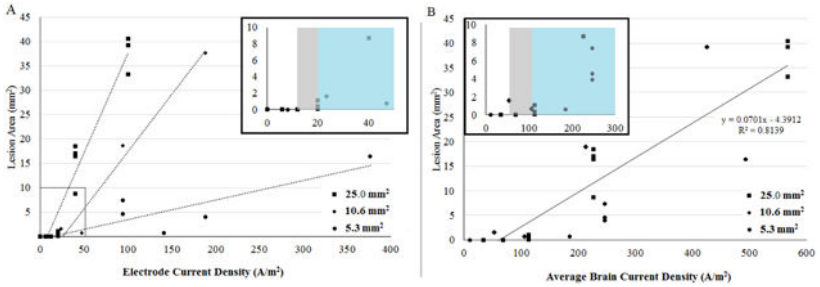

Figure 4.

Effect of electrode current density and brain current density on total brain lesion area. Electrode size was found to be a relevant variable when measuring tissue lesion obtained from brains stimulated at different current densities. **A.** Larger electrodes induced more lesion at similar electrode current densities. **B**. Across electrode sizes, cortical lesion was related to predicted brain current density (R = 0.8139).

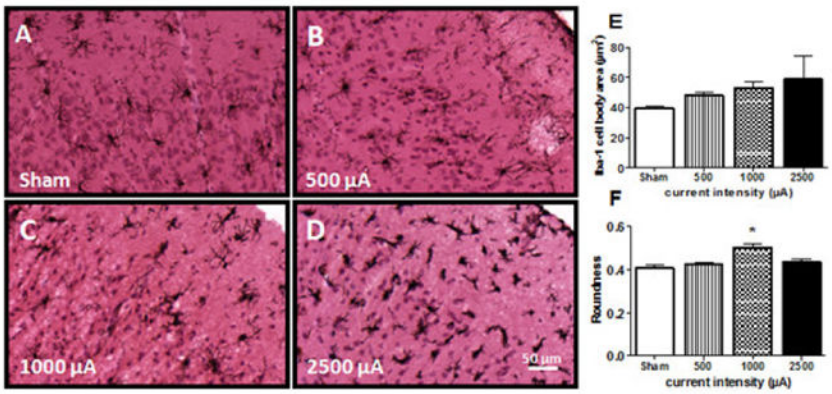

Figure 5.

Micrograph representation (10×) of Iba1 immunoreactive microglia counterstained with H&E in brain sections from sham (A) or tDCS groups at different current intensities: 0.5 mA (B), 1.0 mA (C) and 2.5 mA (D). Cell body area (E) and roundness (F) were additionally measured and quantified to assess lesion-induced changes in microglial morphology. Immunostaining was digitally quantified by Olympus CellSens Dimension software and no differences were observed in the percentage of positive area for Iba1 positive microglia (E).

Table 1

Animal		Anode			Cathode			Lesion
Number	*Stimulation (mA)*	*Electrode*	*Size (mm^2)*	*Placement (mm Bregma)*	*Electrode*	*Size (cm^2)*	*Placement*	*Area (mm^2)*
3	Sham	ValuTrode	25.0	0	ValuTrode	8.04	Back	0
4	0.15							0
4	0.3							0
3	0.5							0.35
								1.08
								0.05
4	1							16.40
								17.05
								8369
								18.49
3	2.5							33.21
								39.20
								40.50
1	Sham	DIXI	10.6	-2.5, 2.5 Bilateral	Ag Ring	0.10	Chest	0.00
1	0.25							1.60
1	0.5							0.70
1	1							18.56
1	2							37.58
1	Sham	DIXI	5.3	-2.5, 2.5 Left	Ag Ring	0.10	Chest	0.00
1	0.043							0.00
2	0.5							4.58
								7.40
1	0.75							0.64
1	1							3.92
1	2							16.41

Table 2

Animal (n)	Stimulation (mA)	Size (mm ^{2})	Stimulation Duration (seconds)	Current Density (A/m ^{2})	Charge (C)	Charge Density (kC/m2)	Lesion Area (mm ^{2})
3	Sham	25	3600				0
4	0.15			6	0.54	21.6	0
4	0.3			12	1.08	43.2	0
3	0.5			20	1.8	72.0	0.35
							1.08
							0.05
4	1			40	3.6	144.0	16.4
							17.05
							8.69
							18.49
3	2.5			100	9	360.0	33.21
							39.2
							40.5
1	Sham	10.6	3600				0
1	0.25			23.5	0.9	84.7	1.6
1	0.5			47.1	1.8	169.5	0.7
1	1			94.2	3.6	339.0	18.56
1	2			188.3	7.2	678.0	37.58
1	Sham	5.3	3600				0
1	0.043					29.2	
2	0.5			94.2	1.8	339.0	4.58
							7.4
1	0.75			141.2	2.7	508.5	0.64
1	1			188.3	3.6	678.0	3.92
1	2			376.6	7.2	1,356.0	16.41